Available online at www.sciencedirect.com
ScienceDirect
Journal of the European Ceramic Society 27 (2007) 223–230
www.elsevier.com/locate/jeurceramsoc

Indentation modulus and hardness of Pb(Zr, Ti)O_3 sol–gel films deposited on Pt and $LaNiO_3$ electrodes An estimation of the C_{ij}^D compliances

P. Delobelle [a,*], G.S. Wang [b], E. Fribourg-Blanc [b], D. Remiens [b]

[a] *Institut FEMTO-ST, UMR CNRS 6174, Laboratoire de Mécanique Appliquée R. Chaléat, Université de Franche-Comté, 24 Chemin de l'Epitaphe, 25000 Besançon, France*

[b] *Matériaux et Intégration pour la Microélectronique et les Microsystèmes, DOAE/IEMN UMR CNRS 8520, Université de Valenciennes et du Hainaut Cambrésis, Z.I. de la petite Savate, 59600 Maubeauge, France*

Received 4 March 2006; received in revised form 18 May 2006; accepted 25 May 2006
Available online 7 August 2006

Abstract

Sol–gel PZT thin films with different crystalline orientations function of the deposit parameters such as: the nature (TiO_x/Pt or $LaNiO_3$) and the thickness of the bottom electrodes, the nature of the precursor solutions and the thickness of the final films, have been fabricated. These parameters affect the crystallite orientations, which has been determined by X-ray diffraction. Nano-indentation tests coupled with continuous stiffness method allowed to obtain the indentation elastic modulii measured under load $M_{\langle hkl\rangle}$ or at almost null load $M_{o\langle hkl\rangle}$ (that is when the ferroelectric domains are or are not oriented with the stress) and the hardness $H_{b\langle hkl\rangle}$ of these ceramics. From the present study and from the literature, the mechanical properties of these films are shown dependent on the crystalline orientation. A compilation of all the reported data allows values of $M_{\langle hkl\rangle}$, $M_{o\langle hkl\rangle}$ and $H_{b\langle hkl\rangle}$ to be proposed for the three characteristic orientations (0 0 1), (1 1 1) and (1 1 0). From these values and acoustic pico-second experiments, possible values of C_{ij}^D and $C_{o_{ij}}^D$ have been proposed.
© 2006 Elsevier Ltd. All rights reserved.

Keywords: PZT; Hardness; Compliances

1. Introduction

Lead zirconate titanate (PZT) thin films are intensively studied for their potential as actuator and sensor in Microsystems. As PZT thin film material is mature and presents among the highest piezoelectric coefficient, its electromechanical properties in thin film form have been investigated for several years.[1] However, for thin films on a thick substrate, the piezoelectric coefficient of interest, i.e., $d_{33,\text{eff}}$ for transverse effect and $d_{31,\text{eff}}$ for transverse-plane effect, are dependent on material mechanical properties,[1,2] due to the plane stress state. Therefore, in order to understand factors acting on these piezoelectric coefficients, the study of the mechanical properties of these thin films seems to be interesting.

PZT films were the subject of few mechanical characterizations.[3–8] Piezoelectric measurements on PZT films are extending but results largely vary according to processing conditions and methods of measurement.[9–11] From our point of view, it is necessary, at this point, to understand whether mechanical behaviour of the film may influence measured values of piezoelectric coefficients. This may be true for transverse piezoelectric coefficient, but also for transverse-plane coefficient. Therefore, mechanical data on our films have been sought in order to be able to better design them for various applications. Nowadays, bulk properties are used by all authors in their design calculations.[2,12]

Several methods have already been published in order to assess mechanical properties of thin films. Among them, impulse acoustic method,[13–15] atomic force microscopy,[16] Brillouin light scattering[17] are reported as well as nano-indentation[18–20] as the most developed methods. It should be noted that few studies were published related to piezoelectric ceramics investigation by nano-indentation.[4–8] The complex behaviour of ferroelectric materials requires a first understanding before going to com-

* Corresponding author. Tel.: +33 381 66 60 13; fax: +33 381 66 67 00.
E-mail address: patrick.delobelle@univ-fcomte.fr (P. Delobelle).

0955-2219/$ – see front matter © 2006 Elsevier Ltd. All rights reserved.
doi:10.1016/j.jeurceramsoc.2006.05.095

Table 1
Summary of the deposit parameters (electrode nature (PZT or LNO), electrode thickness e_s, sub-layer thickness e_{ff}, number of layers n, film thickness e_f, crystallite orientations $\langle h\,k\,l\rangle$, XRD shown in Fig. 1)

Specimen number	Electrode	e_s (nm)	e_{ff} (nm)	n	e_f (nm)	Pronounced orientation	Fig. 1
1	LNO	60	100	10	1000	⟨0 0 1⟩	
2	LNO	90	100	10	1000	⟨0 0 1⟩	
3	LNO	120	100	10	1000	⟨0 0 1⟩	
4	LNO	150	100	10	1000	⟨0 0 1⟩	
5	LNO	180	100	10	1000	⟨0 0 1⟩	Part c
6	LNO	180	100	5	500	⟨0 0 1⟩	
7	LNO	180	100	15	1500	⟨1 1 0⟩ ⟨0 0 1⟩	
8	LNO	180	100	20	2000	⟨1 1 0⟩ ⟨0 0 1⟩ ⟨1 1 1⟩	
9	LNO	180	200	5	1000	⟨1 1 0⟩ ⟨0 0 1⟩ ⟨1 1 1⟩	
10	LNO	180	200	19	3800	⟨1 1 0⟩ ⟨1 1 1⟩	Part b
11	Pt	150	200	8	1600	⟨1 1 0⟩ ⟨1 1 1⟩ ⟨0 0 1⟩	Part d
12	Pt	150	100	12	1200	⟨1 1 1⟩	Part a

plicated methods. For this reason, nano-indentation technique seems to be interesting because it shows a high sensitivity and does not need an extensive modelling at least for isotropic materials.

In this study, the mechanical properties of sol–gel PZT thin films have been evaluated through nano-indentation testing. It has recently been shown that the measure of the true Young modulus of PZT thin films $M_{o\langle h\,k\,l\rangle}$ is possible through nano-indentation test.[7] Here, the biaxial elastic modulii $M_{\langle h\,k\,l\rangle}$, $M_{o\langle h\,k\,l\rangle}$ and the hardness $H_{b\langle h\,k\,l\rangle}$ have been measured by means of a nano-indenter II^S following the protocol developed by Oliver and Pharr.[18–20] This article analyses the transverse mechanical behaviour of sol–gel thin films materials as a function of the deposit parameters such as the nature and the thickness of the bottom electrodes, the number and the thickness of the layers, the nature of the precursor solutions. These parameters affect the crystallographic orientation of the PZT. Table 1 gives information about the deposited films.

2. Experimental procedures

2.1. Thin films

The PZT films are deposited on Si/SiO_2/TiO_x/Pt and Si/SiO_2/LNO. The TiO_x/Pt electrodes are obtained by rf sputtering, the titanium oxide deposition conditions are optimized in order to control the oxidation degree of TiO_x (reactive sputtering); the main objective is to limit the diffusion of Ti across the platinum joint grain. The platinum layers are dense (low deposition rate) to suppress also the possible diffusion of Ti. A post-annealing treatment of the electrodes is made to stabilize the structure.[21,22]

The thickness of TiO_x and Pt are 15 and 150 nm, respectively, the Pt film presents a (1 1 1) preferred orientation. The PZT films deposited on this type of electrode are (1 1 1) oriented whatever the deposition technique (sol–gel or sputtering[8]). The film orientation is related to the film thickness. When the film thickness increases the structure becomes more polycrystalline (Table 1).

The $LaNiO_3$ (LNO) electrodes were prepared by a modified metalloorganic decomposition process, the starting materials were lanthanum acetate and nickel acetate.[21,22] The LNO films were prepared by spinning the precursor solution on SiO_2/Si substrate at 3000 rpm for 30 s. Each annealing layer was dried at 200 °C for 180 s, then pre-fired at 400 °C for 180 s and finally annealed at 700 °C for 180 s (rapid thermal annealing). The LNO films are (0 0 1) preferred orientation. In this study the LNO films thicknesses vary from 60 to 180 nm (Table 1).

For PZT films, the starting materials were tri-hydrated lead acetate, zirconium (IV) *n*-propoxide, and titanium isopropoxide. The precursor solutions were prepared with Zr/Ti ratio of 53/47, and 15% mole excess lead was added to the solution to compensate for lead oxide loss in annealing process and to suppress the pyrochlore formation. Two PZT solutions were prepared to obtain different single-thicknesses. One PZT solution (named solution 1) with single-layer thickness about e_{ff} = 100 nm prepared by using 2-methoxyethanol as solvent with concentration of 0.6 M, the other with single-layer thickness about e_{ff} = 200 nm prepared by using acetate acid as solvent with concentration of 0.7 M (named solution 2). Consequently, the PZT thin films were deposited by spinning the solution on LNO or Pt coated Si substrates at 3000 rpm for 30 s. Each layer of the films was dried at 200 °C for 180 s, then pre-fired at 400 °C for 240 s to remove the residual organics, following by a rapid thermal annealed at 650 or 700 °C for 240 s. The different thicknesses of PZT were achieved by repeated the spin-coating and heating treatment cycles. The whole heating treatment was conducted in pure oxygen atmosphere. The PZT film thickness range is from 500 to 3800 nm (Table 1).

Fig. 1 shows the typical X-ray diffraction spectrum of one layer of PZT films deposited on Pt electrode; for solution 1 (Fig. 1a) the film is perfectly (1 1 1) oriented, but for solution 2 (Fig. 1b) the film is polycrystalline; the (1 1 0) orientation is more pronounced. For PZT films deposited by sputtering on platinum electrode, we have observed the same structural evolution (1 1 1) for films thinner than 0.5 μm and a trend to develop a polycrystalline film for thicker film. This effect is well known, when the film thickness increases, the structure tends to a polycrystalline structure (except for epitaxial growth). For the PZT films deposited on LNO electrodes the behaviour is quite similar. A well oriented (0 0 1) for one layer of solution 1 (Fig. 1c) and polycrystalline with (1 1 0) preferred orientation for solution 2 (Fig. 1d).

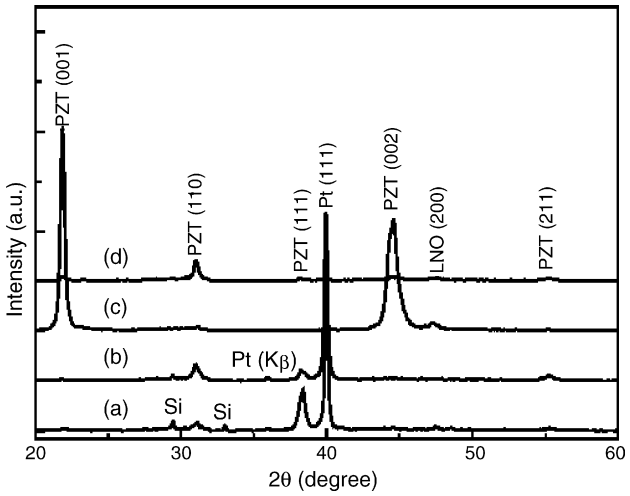

Fig. 1. XRD of PZT deposited on: (a) Pt with single layer thickness of 100 nm, (b) Pt with layer of 200 nm, (c) LNO with layer of 100 nm and (d) LNO with layer of 200 nm.

The grain size of (1 1 1) PZT oriented and (0 0 1) PZT oriented is similar; values of 50–80 nm have been measured. For polycrystalline films, i.e. (1 1 0) oriented, the grain size is larger. The R_{ms} roughness values for PZT in area of 10 μm × 10 μm are about 2.5, 3.7 and 4.2 nm for (0 0 1), (1 1 1) and a mixing of (1 1 0) or (1 1 1) and (0 0 1) orientations, respectively.

2.2. Nano-indentation measurements

Nano-indentation tests were performed using a nano-indenter II^S (Nano-Instruments) using the continuous stiffness method (CSM). Nano-indentation consists in performing, through a predefined and controlled loading path, the penetration of a diamond tip in the sample material under test. We used here a common Berkovich tip (tetrahedron).

In nano-indentation, the $M_{\langle h\,k\,l\rangle}$ modulus, measured on a single crystal, whose normal to the surface has director cosine α_i is given by[23,24]:

$$M_{\langle h\,k\,l\rangle} = 16\pi^2 \left[\int_0^{2\pi} \alpha_m \beta_{km}^{-1}(\gamma)\alpha_k \,\mathrm{d}\gamma\right]^{-1} \quad \text{with}$$

$$M_{\langle hkl\rangle} = \left[\frac{1}{M_r} - \left(\frac{1-\nu^2}{E}\right)_{\mathrm{ind}}\right]^{-1} \quad \text{and} \quad M_r = \frac{\sqrt{\pi}}{2\beta\sqrt{A}}\frac{\mathrm{d}P}{\mathrm{d}h},$$

$$A(h_c) = 24.5h_c^2 + \sum_{n=1}^{4}(a_n h_c^{1/n}), \quad h_c = h - \varepsilon\left(\frac{P}{S}\right). \qquad (1)$$

A is the projected contact area, P the applied load, $S = (\mathrm{d}P/\mathrm{d}h)$ the unloading stiffness measured at the depth of penetration h, $\beta = 1.034$ and $\varepsilon = 0.72$ for the Berkovich's tip. $(E/1-\nu^2)_{\mathrm{ind}}$ is the reduced modulus of the diamond indenter, γ the angle in surface plane and $\beta_{km}(\gamma)$ a complicated matrix function of the compliance C_{ij} and γ.[24]

In this case, depending on the crystallite orientation occurring in the deposition process as mentioned before, the $M_{\langle h\,k\,l\rangle}$ modulus determined by nano-indentation should not be constant. The measured hardness is given by:

$$H_{\mathrm{b}\langle h\,k\,l\rangle} = \frac{P}{A}. \qquad (2)$$

The study was conducted under the continuous contact stiffness measurement procedure[18] with a frequency of 45 Hz and an indenter vibration amplitude of 1 nm during penetration of the tip in the sample.

For each tested sample the measurement sequence consists in 15 indents with a 50 μm space between them, on 2 different places (15 × 2), and for a maximum depth $h_{max} = 320$ nm covering then a 200 μm × 200 μm area. The penetration speed was not constant but increased with the depth penetration from 1 to 8 nm s^{-1}

Moreover, on each film, a repeated progressive loading was done with keeping the load during one minute at the highest level. The maximum values of the load were 0.2, 0.5, 1 mN and 90% of unloading was performed. This kind of loading, with the total control of the load, let, on one hand, ensure the contact between the indenter and the film during the whole loading–unloading sequence, and on the other hand, estimate the average thermal drift during the maintenance of a constant load and thus to correct its effect on the measurements. This kind of loading allows to determine not only the $M_{\langle h\,k\,l\rangle}$ modulus but also the $M_{\mathrm{o}\langle h\,k\,l\rangle}$ modulus at almost null load, i.e., when the ferroelectric domains are not subjected to the indenter pressure.[7]

3. Experimental results

On each tested film, a small discontinuity is observed in the loading part of the curve $P = f(h)$, which should be a sign for the occurrence of micro-cracks. Indeed, cracks are optically revealed after the indentation test, which is in agreement with the observations of Bahr et al.[4] and Zheng et al.[5] The depth h_r at which these discontinuities appear is in the range of 70–120 nm. This is still in agreement with the reported analysis where this phenomenon seems to occur only for depths greater than 100 nm.[4] So the measured values of the elastic modulus and of the hardness below h_r are not subject of any artefact.

3.1. Indentation modulus $M_{\langle h\,k\,l\rangle}$ and hardness $H_{b\langle h\,k\,l\rangle}$ of the thin films

In order to study the evolution of $M_{\langle h\,k\,l\rangle}$ and $H_{\mathrm{b}\langle h\,k\,l\rangle}$ with the micro-structural parameters of the studied films, taking into account the presence of the substrate, the analyse of measurements at low indentation depths, typically for $h/e_f \leq 10\%$[25–27] is required. Thus, results are analysed for $h/e_f = 2.5$, 5 and 10%. Taking account for values of e_f, the studied indentation depth is included between 12 and 300 nm. However, the only values calculated for $h < h_r$ are not subjected to the micro-cracks occurrence.

The measured values of $M_{\langle h\,k\,l\rangle}$ for the lowest depths (20 nm < h < 50 nm) present a high standard deviation σ_E since the roughness R_{ms} is included between 2.5 and 4.2 nm. The ratio σ_E/E_{mean}, where E_{mean} is the mean value of the Young's modulus of an isotropic material, is obviously an increasing function

Table 2
Theoretical and experimental estimations of the relative standard deviation at $h = 25$ and 50 nm for different crystalline orientations

Orientation	R_{ms} (nm)	$(\sigma_E)/(E_{mean})$ (%) at $h = 25$ nm		$(\sigma_E)/(E_{mean})$ (%) at $h = 50$ nm		$M_{\langle hkl\rangle}$ (GPa)
		Theoretical	Experimental	Theoretical	Experimental	
⟨0 0 1⟩	2.5	7.9	6.3 ± 1.2	5.1	4.1 ± 0.7	180 ± 5
⟨1 1 1⟩	3.7	10.2	10.9 ± 1.4	6.5	7.5 ± 1.4	156 ± 8
⟨1 1 0⟩ ⟨1 1 1⟩ ⟨0 0 1⟩	4.2	11.1	15.6 ± 5.1	7.1	10.1 ± 2.1	125 ± 8

of R_{ms}, a decreasing function of the indentation depth h and, according to the dimensionless parameter R_{ms}/h the following equation can be written[28–30]:

$$\frac{\sigma_E}{E_{mean}} = \alpha\left(\frac{R_{ms}}{h}\right)^m \quad \text{with} \quad h = pe_f$$
$$\text{and} \quad p = 2.5\,,\,5 \text{ or } 10\%. \tag{3}$$

σ_E, the standard deviation, is measured over more than 25 indents.[28] Exponent m is a slightly decreasing function of the roughness fractal D. For many metallic films deposited by sputtering technique and for the ceramic films, α and m have already been identified[30]: $\alpha = 0.346$ and $m = 0.64$.

Table 2 gives the results, applying Eq. (3), for $h = 25$ and 50 nm ($h/e_f = 2.5$ and 5% for $e_f = 1000$ nm) according to the values of R_{ms} for the different orientations. These values are compared to the experimental ones calculated with $E_{mean} = M_{\langle hkl\rangle mean}(1 - \nu^2)$ with $\nu = 0.28$. For well-oriented crystallites (0 0 1) and (1 1 1) orientations, there is a fairly good agreement between the calculated and the experimental values. However, for polycrystalline films, with simultaneous (1 1 0) (1 1 1) (0 0 1) orientations, the experimental values are greater than those estimated with Eq. (3). As a result, the relative standard deviation $(\sigma_E)/(E_{mean}) = (\sigma_E/(1 - \nu^2)\, M_{\langle hkl\rangle mean})$ can be considered as an indicator of the degree of the crystallite disorientation. More the disorientation, greater the standard deviation. This observation is in agreement with the Wang et al.[6] analysis.

Figs. 2 and 3 present the evolutions of the $M_{\langle hkl\rangle}$ modulus and the hardness $H_{b\langle hkl\rangle}$ versus the films thickness e_f (lower scale) and the LNO electrode thickness e_s (upper scale) for the two precursor solutions (solutions 1 and 2) and for $h/e_f = 2.5$, 5 and 10%. The measured values obtained for Pt electrode are also reported. The different solid curves correspond to $h/e_f = 5\%$.

The PZT having a tetragonal or rhombohedral symmetry and nano-indentation being sensitive to the crystalline structure orientation (Eq. (1)), the measured $M_{\langle hkl\rangle}$ modulus is expected to depend on the columnar orientation, which is not compulsory the case for the hardness. The $M_{\langle hkl\rangle}$ modulus is found between 140 and 188 GPa, and the hardness between 6 and 9.5 GPa.

Notice that the thickness of the LNO electrode has no influence on the $M_{\langle hkl\rangle}$ and $H_{b\langle hkl\rangle}$ values (Figs. 2 and 3), the films thickness being constant and equal to 1000 nm with $n = 10$ (solutions 1). All these films present a very well (0 0 1) oriented structure (Table 1). Thus, we can conclude that $M_{\langle 0\,0\,1\rangle} = 184 \pm 6$ GPa and $H_{b\langle 0\,0\,1\rangle} = 8.6 \pm 0.6$ GPa. These two values are greater than those determined on thin sputtered films whose orientations are (1 1 1) and (1 1 0).[8]

For the two films deposited on Pt electrode, the first one manufactured with the precursor 1 is perfectly (1 1 1) oriented, and the second one, obtained with the precursor 2, presents a more polycrystalline texture, the (1 1 0) orientation being more pronounced.

From these observations and according to Figs. 2 and 3, $M_{\langle 1\,1\,1\rangle}$ is proposed to be equal to 159 ± 10 GPa and $H_{b\langle 1\,1\,1\rangle}$ to 7.5 ± 0.6 GPa. Note that these two values are close to those determined on sputtered films for the same (1 1 1) orientation.[8]

The other films deposited on LNO show multiple crystallographic orientations. Classified by decreasing X-rays intensity, the following orientations are observed (1 1 0) (0 0 1) (0 0 2) (1 1 1) (1 1 2). The (1 1 0) direction is always the more pronounced. On these four films, as a first approximation, the

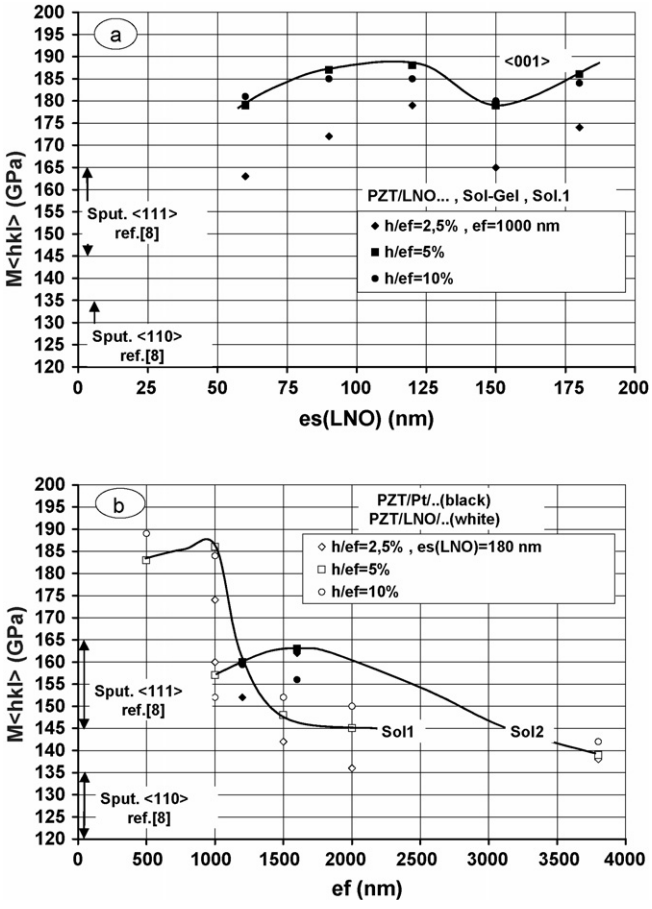

Fig. 2. Evolution of $M_{\langle hkl\rangle}$ modulus as a function of: (a) the electrode thickness (e_s) (in this case $e_f = 1000$ nm), (b) the film thickness (e_f) (in this case e_s(LNO) = 180 nm) for the two precursor solutions (solutions 1 and 2) at $h/e_f = 2.5$, 5 and 10%. The results obtained with Pt electrode are also reported.

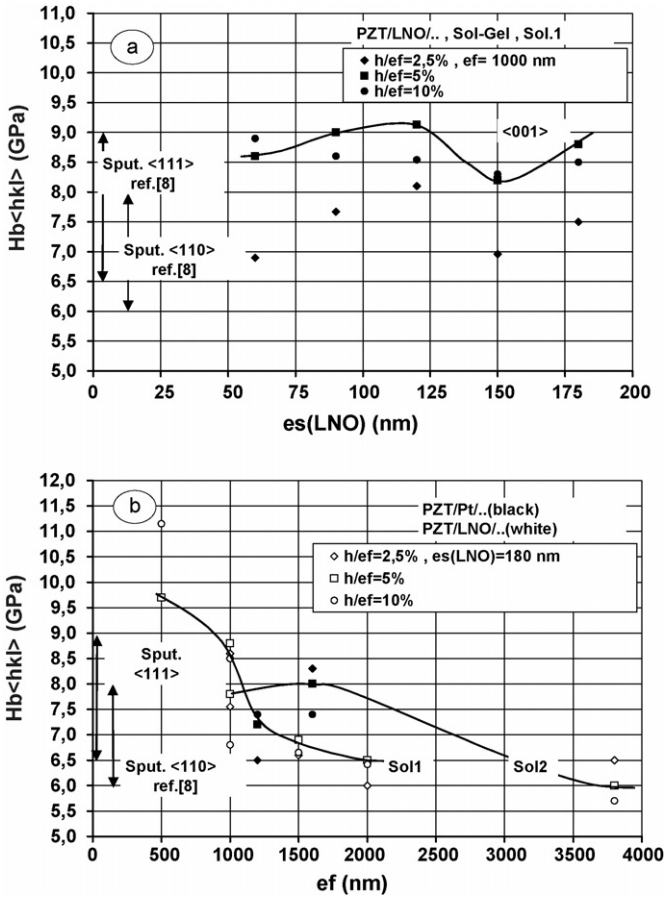

Fig. 3. Evolution of hardness $H_{b\langle hkl\rangle}$ as a function of: (a) the electrode thickness (e_s) (in this case $e_f = 1000$ nm), (b) the film thickness (e_f) (in this case e_s(LNO) = 180 nm) for the two precursor solutions (solutions 1 and 2) at $h/e_f = 2.5$, 5 and 10%. The results obtained with Pt electrode are also reported.

percentage of the crystallite orientation in the same direction is given by the relative height of the diffraction peak in this direction (more precisely by the full width at half maximum), so a linear mixture law on the moduli for the three (0 0 1) (1 1 0) (1 1 1) directions can be used, and thus, it becomes possible to estimate the $M_{\langle 1\,1\,0\rangle}$ modulus. Taking into account the previously $M_{\langle hkl\rangle}$ measured values, $M_{\langle 0\,0\,1\rangle} = 184$ GPa and $M_{\langle 1\,1\,1\rangle} = 159$ GPa, a value of $M_{\langle 1\,1\,0\rangle} = 118 \pm 18$ GPa is deduced. The hardness is of the order of $H_{b\langle 1\,1\,0\rangle} = 6.3 \pm 0.6$ GPa. These values are in range of those determined on sputtered films with (1 1 0) preferred orientation, $M_{\langle 1\,1\,0\rangle} = 126 \pm 6$ GPa and $H_{b\langle 1\,1\,0\rangle} = 7.0 \pm 1.0$ GPa.[8]

Moreover, globally and independently of the nature of the precursor, the $M_{\langle hkl\rangle}$ (and $H_{b\langle hkl\rangle}$) values are reported as decreasing functions of the films thickness. In fact, the preferred orientation given by the nature of the bottom electrode ((0 0 1) for LNO and (1 1 1) for Pt) is progressively lost when the films thickness increases and evolves towards a more isotropic texture. For an hexagonal crystallographic symmetry, applied to bulk PZT ceramics,[8] the following inequality has been shown:

$$M_{\langle 1\,0\,0\rangle} = M_{\langle 1\,1\,0\rangle} < \frac{E}{1-\nu^2} < M_{\langle 1\,1\,1\rangle} < M_{\langle 0\,0\,1\rangle}. \quad (4)$$

Thus, this inequality correlated with the crystallites orientation explains the $M_{\langle hkl\rangle}$ modulus decreasing as a function of the films thickness.

At last, for the same film thickness ($e_f = 1000$ nm in Fig. 2), the modulus corresponding to the precursor 2 is lower than those relative to precursor 1.

Indeed, with the precursor 2, when the sub-layer thickness is increasing ($e_{ff} = 200$ nm), a more disoriented texture is observed. Thus, at constant film thickness, the final orientation of the film is influenced by the sub-layer thickness.

3.2. Indentation modulus $M_{o\langle hkl\rangle}$ at null pressure

For a (0 0 1) oriented film, Fig. 4 gives an example of the indentation curve $P = f(h)$ for a loading–unloading sequence (a) and the evolution of the indentation elastic modulus versus the indentation depth (b) for the four consecutive paths ($P_{max} = 0.2$, 0.5, 1 mN and a time-delay in which the load is maintained at 1 mN). This figure points obviously out that there is a strong evolution of the elastic modulus versus the applied force conversely to non-ferroelectric materials.[7,8] In case of ferroelectric–ferroelastic material, a simple explanation can be found. Indeed, ferroelectric materials, such as PZT, present polarization domains, which are very sensitive to pressure. This is the main reason why care is required when using these materials, which may loose their properties

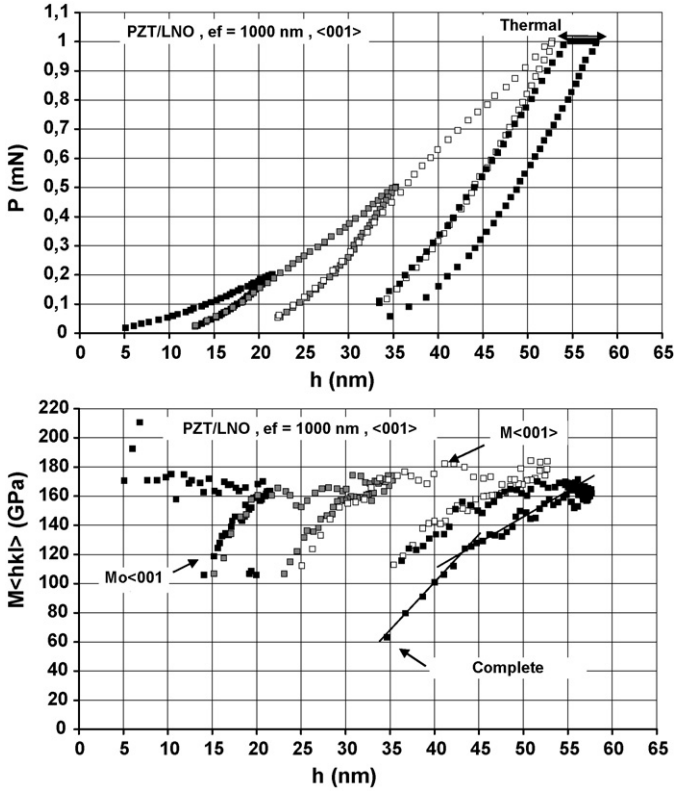

Fig. 4. (a) Tip force vs. indentation depth during a repeated progressive loading ($P_{max} = 0.2$, 0.5, 1 mN) and for a time-delay (1 min) in which the load is maintained constant ($P_{max} = 1$ mN) and (b) elastic modulus as a function of the indentation depth during a full indentation sequence, determination of $M_{\langle hkl\rangle}$ and $M_{o\langle hkl\rangle}$.

by depoling under strong pressure.[31] Then, during indentation, the different loading–unloading paths can be described from the point of view of the movements of ferroelectric domains. At the first loading curve, the modulus values are a little scattered because of the surface roughness, which introduces some uncertainty on the depth measurement. A plateau is reached, which is equivalent to a saturation of the ferroelectric domains all oriented in the same direction, function of the indenter geometry. The material is hardened, which allows the determination of the $M_{\langle hkl\rangle}$ modulus. At the release of the force during unloading, the ferroelectric domains recover their initial state so that the material shows a decrease of its elastic modulus.[7,8] So, the lowest modulus values in these representations, corresponding to 90% of unloading, allow the $M_{o\langle hkl\rangle}$ determination. From several films having different orientations; PZT(0 0 1)/LNO, PZT(1 1 1)/Pt and polycrystalline with (1 1 0) preferred orientation, the following values have been determined: $M_{o\langle 1\,1\,0\rangle} = 94 \pm 12$ GPa, $M_{o\langle 1\,1\,1\rangle} = 106 \pm 12$ GPa and $M_{o\langle 0\,0\,1\rangle} = 120 \pm 13$ GPa. These values are in the range of those determined on sputtered films with (1 1 0) and (1 1 1) orientations[8]; $M_{o\langle 1\,1\,0\rangle} = 89 \pm 5$ GPa and $M_{o\langle 1\,1\,1\rangle} = 102 \pm 10$ GPa.

3.3. Acoustic pico-second experiments

An acoustic pico-second experiment was done at the IEMN[15,32] on a PZT film, only one layer of 1073 nm thick (1 1 0) oriented. For this method, ultrasonics ultra-short optical pulses are used in a pump and probe scheme to make ultrasonic measurements at very high frequency (up to several hundred GHz). This experiment gave the sound velocity in the material, i.e., $V = 4750\ \mathrm{m\,s^{-1}}$. It is known that:

$$V = \sqrt{\frac{f(C_{ij})}{\rho}} \tag{5}$$

Presently, for an (1 1 0) orientation (also for (1 0 0)), $f(C_{ij}) = C_{11}^D$. A density of $7500\ \mathrm{kg\,m^3}$ gives $C_{11}^D = 169 \pm 10$ GPa. Table 3 reports the values of the compliances C_{ij}^D at constant polarisation of soft and hard PZT ceramics.[33] The values of C_{11}^D are respectively of 160.6 and 147.8 GPa. In this case, the measured value is close to the C_{11}^D compliance of hard ceramic.

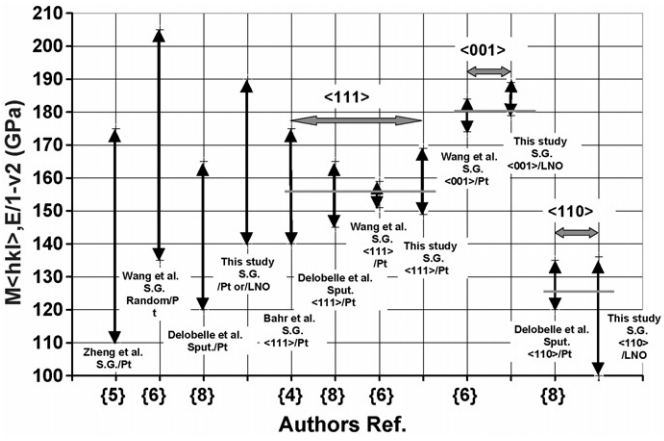

Fig. 5. Summary of the $M_{\langle hkl\rangle}$ values reported from the literature and this study. Propositions for the $M_{\langle 0\,0\,1\rangle}$, $M_{\langle 1\,1\,0\rangle}$, and $M_{\langle 1\,1\,1\rangle}$ values.

4. Discussion

From the literature[4–6,8] and the present study, Fig. 5 shows synthesis of the $M_{\langle hkl\rangle}$ values (or $E/1-\nu^2$ when no indication about the crystallite orientation is known) obtained on thin PZT films manufactured with sputtering or sol–gel methods and deposited on Pt or LNO electrodes. The results are very scattered and the maximum $M_{\langle hkl\rangle}$ range is $110\ \mathrm{GPa} < M_{\langle hkl\rangle} < 205\ \mathrm{GPa}$. However, when the crystallites orientation is known (Refs. 4,6,8 and this study), there is a fairly good correlation between the value of the indentation modulus and the crystallites orientation imposed by the deposit parameters. Finally, for the three characteristic orientations, the proposed mean values are:

$$M_{\langle 0\,0\,1\rangle} = 180 \pm 5\ \mathrm{GPa}, \qquad M_{\langle 1\,1\,1\rangle} = 156 \pm 8\ \mathrm{GPa},$$

$$\text{and} \quad M_{\langle 1\,1\,0\rangle} = 125 \pm 10\ \mathrm{GPa}$$

Moreover, for the indentation modulus $M_{o\langle hkl\rangle}$ at low stress, the proposed mean values are:

$$M_{o\langle 0\,0\,1\rangle} = 120 \pm 13\ \mathrm{GPa}, \qquad M_{o\langle 1\,1\,1\rangle} = 102 \pm 10\ \mathrm{GPa},$$

$$\text{and} \quad M_{o\langle 1\,1\,0\rangle} = 89 \pm 6\ \mathrm{GPa}$$

As far as the hardness is concerned, the data are more scattered, but the following values can be proposed:

Table 3
Values of the compliances C_{ij}^D for soft and hard bulk PZT

C_{ij}^D (GPa)	Soft bulk PZT	Hard bulk PZT	Thin film, C_{ij}^D	Thin film, $C_{o_{ij}}^D$
C_{11}^D	147.8	160.6	169	148
C_{12}^D	106.7	89.2	109	107
C_{13}^D	79.9	65.1	65	80
C_{33}^D	153.8	165	219	169
C_{44}^D	37.8	62.3	62.3	37.8
C_{66}^D	20.5 (20.55)	35.7 (35.7)	30	20.5
$M_{\langle 0\,0\,1\rangle}$	112 (c)	149 (c)	180 (m)	120 (m)
$M_{\langle 1\,1\,0\rangle}$	89 (c)	129 (c)	125 (m)	89 (m)

Possible values of C_{ij}^D and $C_{o_{ij}}^D$ determined in this study for thin films. Values of calculated (c) and measured (m) moduli $M_{\langle hkl\rangle}$ and $M_{o\langle hkl\rangle}$.

$H_{b\langle 0\,0\,1\rangle} = 8.6 \pm 0.6\,\text{GPa}$, $H_{b\langle 1\,1\,1\rangle} = 7.7 \pm 0.7\,\text{GPa}$, and $H_{b\langle 1\,1\,0\rangle} = 6.3 \pm 0.6\,\text{GPa}$

If the same experimental sequence of nano-indentation on hard and soft bulk PZT ceramics is performed,[34] the respectively high and low biaxial moduli $E/1-\nu^2$, 152/106 and 122/73 GPa are obtained. Moreover, a compressive test on those same bulk ceramics leads respectively below the coercive stress to $E/1-\nu^2 = 108\,\text{GPa}$ ($E = 93\,\text{GPa}$, $\nu = 0.38$) and 77 GPa ($E = 65\,\text{GPa}$, $\nu = 0.4$).[34,35] These values correspond to those obtained from nano-indentation under low load, which means that the elastic modulus, without any reorientation of the domains, is the one obtained at low load below the coercive stress. Notice that, the moduli at saturation in compressive test (i.e., for stresses higher than three time the coercive stress) are respectively for hard and soft bulk ceramics 159 and 129 GPa. These values are close to those obtained from nano-indentation test under load. Once more, the measured values on the thin films are closer to those of hard bulk ceramic than to those of soft ceramic. For isotropic material the upper and lower biaxial moduli should be in the order of $M_{\langle 1\,1\,1\rangle}$ and $M_{o\langle 1\,1\,1\rangle}$, respectively.

As previously mentioned, the PZT having a tetragonal (or rhombohedra) symmetry and nano-indentation being very sensitive to the crystalline orientation (Eqs. (1) and (2)), the measured modulus $M_{\langle h\,k\,l\rangle}$ depends on the columnar orientation.[23] No general analytic solution of Eq. (1) exists. However, for some configurations, approximate solutions are available and give very close results to numerical solutions resulting from Eq. (1).

The actual symmetry is tetragonal thus $C_{66} \neq (C_{11} - C_{12})/2$, but from a quantitative point of view the C_{ij}^D compliances values given in Table 3[33] verify at less than 1% the relation $C_{66} = (C_{11} - C_{12})/2$ (values in parentheses). Thus, an hexagonal symmetry can be considered for the different calculations. For this symmetry (isotropic transverse) it is shown[36] that:

$$M_{\langle 0\,0\,1\rangle} = \frac{2}{\sqrt{\frac{C_{11}}{C_{11}C_{33}-C_{13}^2}/\left(\frac{1}{C_{44}} + \frac{2}{\sqrt{C_{11}C_{33}}+C_{13}}\right)}} \quad (6)$$

and

$$M_{\langle 1\,0\,0\rangle} = M_{\langle 1\,1\,0\rangle} = \sqrt{\frac{C_{11}^2 - C_{12}^2}{C_{11}}\sqrt{\frac{C_{11}}{C_{33}}}M_{\langle 0\,0\,1\rangle}}. \quad (7)$$

Between these two values, it does not exist any solution. An estimate solution can be calculated, applying Eq. (7) to the average values of the compliances $\langle C_{ij}^* \rangle$ obtained by integration in the normal plan of the indentation direction of the compliances C_{ij}^* expressed also in this same direction.[8] Fig. 6 shows the different experimental values of the indentation moduli ($M_{\langle h\,k\,l\rangle}$, $M_{o\langle h\,k\,l\rangle}$, $E/1-\nu^2$, $E_o/1-\nu^2$) obtained on sol–gel and sputtered thin films,[8] hard and soft bulk ceramic,[34] as well as the theoretical values of $M_{\langle 1\,0\,0\rangle}$, $M_{\langle 0\,0\,1\rangle}$ calculated using Eqs. (6) and (7) with the C_{ij}^D values given in Table 3, as a function of the dihedral angle β of the indentation direction ($\beta = 90^\circ$ corresponds to $\vec{C}$ axis). The continuous approximations $M_{\langle h\,k\,l\rangle}$ using

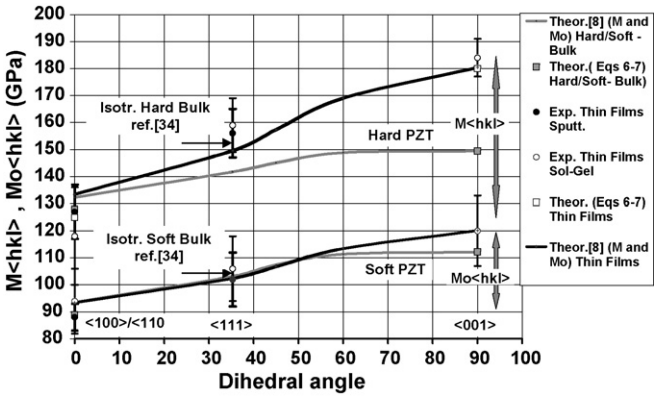

Fig. 6. Evolution of the experimental and theoretical values of $M_{\langle h\,k\,l\rangle}$ and $M_{o\langle h\,k\,l\rangle}$ as a function of the dihedral angle for the thin films and the bulk hard and soft PZT ceramics.

the previous described method are also reported. For $\beta = 0$, the measured moduli on the thin films $M_{\langle 1\,1\,0\rangle}$, $M_{o\langle 1\,1\,0\rangle}$ are respectively close to those calculated for hard and soft bulk PZT. This is no longer the case for $\beta = 90^\circ$ where the moduli of the thin films are greater than those of bulk ceramics. Knowing $M_{\langle 0\,0\,1\rangle} = 180\,\text{GPa}$ and $C_{11}^D = 169\,\text{GPa}$, thanks to relation 6 the variations of $C_{44}^D = f(C_{13}^D)$ for different fixed values of C_{33}^D (with $C_{33}^D \geq C_{11}^D$) have been calculated. Moreover, if we consider that the compliances values C_{13}^D and C_{44}^D on the films are the same than those on hard bulk ceramic, there is only one value of C_{33}^D which verifies Eq. (6). Now, knowing C_{33}^D, C_{11}^D, $M_{\langle 0\,0\,1\rangle}$ and $M_{\langle 1\,1\,0\rangle}$ the value of C_{12}^D is evaluated from Eq. (7). The same way is applied for the low values of the modulus by considering C_{o11}^D equal to C_{11}^D of the soft bulk ceramic. The values of the calculated compliances C_{ij}^D and $C_{o_{ij}}^D$ of the thin films are reported in Table 3. The evolutions of the upper and lower moduli as a function of the dihedral angle and evaluated using the method previously described[8] are drawn in Fig. 6. As it could be expected, the compliance C_{33}^D of these thin films are greater than those of bulk PZT ceramics.

5. Conclusions

In summary, sol–gel PZT thin films with different crystalline orientations function of the deposit parameters (precursor, nature of the bottom electrode, films thickness, etc.) have been manufactured. Nano-indentation tests coupled with continuous stiffness measurements allowed the $M_{\langle h\,k\,l\rangle}$ elastic modulus and the hardness of these ceramic films to be obtained. From the literature and the present study, it is clearly shown that the mechanical properties of these films greatly depend on the crystalline orientation. A compilation of all the reported data leads to propose:

$$M_{\langle 1\,1\,0\rangle} = 125 \pm 10\,\text{GPa} < M_{\langle 1\,1\,1\rangle} = 156 \pm 8\,\text{GPa} < M_{\langle 0\,0\,1\rangle} = 180 \pm 5\,\text{GPa}$$

$$M_{o\langle 1\,1\,0\rangle} = 89 \pm 6\,\text{GPa} < M_{o\langle 1\,1\,1\rangle} = 102 \pm 10\,\text{GPa} < M_{o\langle 0\,0\,1\rangle} = 120 \pm 12\,\text{GPa}$$

and

$$H_{b\langle 1\,1\,0\rangle} = 6.3 \pm 0.6\,\text{GPa} < H_{b\langle 1\,1\,1\rangle} = 7.7 \pm 0.7\,\text{GPa} < H_{b\langle 0\,0\,1\rangle} = 8.6 \pm 0.6\,\text{GPa}$$

From these results and those of some pico-second acoustic experiments, possible values of the compliances C_{ij}^{D} and $C_{o_{ij}}^{D}$ are proposed for the thin PZT films.

These values should be taken into account for the MEMS applications. An other important result is that the use of thick polycrystalline films for MEMS application is not a good challenge, since the mechanical properties are reduce compared with those of well oriented films.

References

1. Lefki, K. and Dormans, G. J. M., Measurement of piezoelectric coefficients of ferroelectric thin films. *J. Appl. Phys.*, 1994, **76**, 1764–1767.
2. Shepard Jr., J. F., Moses, P. J. and Trolier-McKinstry, S., The wafer flexure technique for the determination of piezoelectric coefficient d31 of PZT thin films. *Sens. Actuators A*, 1998, **71**, 133–138.
3. Kanno, I., Fujii, S., Kamada, T. and Takayama, R., Piezoelectric properties of C axis oriented Pb(Zr,Ti)O_3 thin films. *Appl. Phys. Lett.*, 1997, **70**, 1378–1380.
4. Bahr, D. F., Robach, J. S., Wright, J. S., Francis, L. F. and Gerberich, W. W., Mechanical deformation of PZT thin films for MEMS applications. *Mater. Sci. Eng. A*, 1999, **259**, 126–131.
5. Zheng, X. J., Zhou, Y. C. and Li, Y. Y., Nano-indentation fracture test of Pb(Zr,Ti)O_3 ferroelectric thin films. *Acta Mater.*, 2003, **51**, 3985–3997.
6. Wang, Q. M., Ding, Y., Chen, Q., Zhao, M. and Cheng, J., Crystalline orientation dependence of nanomechanical properties of Pb(Zr,Ti)O_3 thin films. *Appl. Phys. Lett.*, 2005, **86**, 162903, 1–3.
7. Delobelle, P., Guillon, O., Fribourg-Blanc, E., Soyer, C., Cattan, E. and Remiens, D., True Young modulus of Pb(Zr,Ti)O_3 films measured by nano-indentation. *Appl. Phys. Lett.*, 2004, **85**(22), 5185–5187.
8. Delobelle, P., Fribourg-Blanc, E. and Remiens, D., Mechanical properties determined by nano-indentation tests of Pb(Zr,Ti)O_3 and Pb(Mg,Nb,TiO_3) sputtered thin films, *Thin Solid Films*, 2006 (on line).
9. Zhang, Q., Pan, W. and Cross, L. E., Laser interferometer for the study of piezoelectric and electrostrictive strains. *J. Appl. Phys.*, 1988, **63**, 2492–2496.
10. Dubois, M. A. and Muralt, P., Measurement of the effective transverse piezoelectric coefficient e31 of AlN and Pb(Zr,Ti)O_3 thin films. *Sens. Actuators A*, 1999, **77**, 106–112.
11. Cattan, E., Haccart, T., Velu, G., Remiens, D., Bergaud, C. and Nicu, L., Piezoelectric properties of PZT films for microcantilever. *Sens. Actuators A*, 1999, **74**, 60–64.
12. Luginbuhl, Ph., Racine, G. A., Lerch, Ph., Romanowicz, B., Brooks, K. G., de Rooij, N. F., Renaud, Ph. and Setter, N., Piezoelectric cantilever beams actuated by PZT sol–gel thin film. *Sens. Actuators A*, 1996, **54**, 530–535.
13. Hurley, D. C., Tewary, V. K. and Richards, A. J., Thin film elastic property measurements with laser ultrasonic SAW spectrometry. *Thin Solid Films*, 2001, **398**, 326–330.
14. Thomsen, C., Grahn, H. T., Tauc, J. and Maris, H. J., Picosecond interferometry technique for study of phonons in the Brillouin frequency range. *Opt. Commun.*, 1986, **60**, 55–58.
15. Devos, A. and Lerouge, C., Evidence of laser wavelength effect in picosecond ultrasonics: possible connection with interband transition. *Phys. Rev. Lett.*, 2001, **86**, 2669–2672.
16. Miyahara, K., Nagashima, N., Ohmura, T. and Matsuoka, S., Evaluation of mechanical properties in nanometer scale using AFM based nano-indentation tester. *Nanostruct. Mater.*, 1999, **12**, 1049–1952.
17. Djemia, P., Dugautier, C., Chauveau, T., Dogheche, E., De Barros, M. I. and Vandenbulck, L., Mechanical properties of diamond films. A comparative study of polycrystalline and smooth fine grained diamonds by Brillouin light scattering. *J. Appl. Phys.*, 2001, **90**, 3771–3779.
18. Oliver, W. C. and Pharr, G. M., An improved technique for determining hardness and elastic modulus using load displacement sensing indentation experiments. *J. Mater Res.*, 1992, **7**, 1564–1583.
19. Pharr, G. M., Oliver, W. C. and Brotzen, F. R., On the generality of the relationship among contact stiffness, contact area, and elastic modulus during indentation. *J. Mater. Res.*, 1992, **7**, 613–617.
20. Oliver, W. C. and Pharr, G. M., Measurement of hardness and elastic modulus by instrumented indentation. Advances in understanding and refinements to methodology. *J. Mater. Res.*, 2004, **19**(1), 3–20.
21. Wang, G. S., Zhao, Q., Meng, X. J., Chu, J. H. and Rémiens, D., Preparation of higly (0 0 1) oriented $LaNiO_3$ nanocrystalline films by metalorganic chemical liquid deposition. *J. Cryst. Growth*, 2005, **277**, 450–456.
22. Wang, G. S., Rémiens, D., Soyer, C., Gogheche, E. and Cattan, E., The effect of $LaNiO_3$ botton electrode thickness on ferroelectric and dielectric properties of (0 0 1) oriented Pb(Zr,Ti)O_3 films. *J. Cryst. Growth*, 2005, **284**, 184–189.
23. Vlassak, J. J. and Nix, W. D., Measuring the elastic properties of anisotropic materials by means of indentation experiments. *J. Mech. Phys. Solids*, 1994, **42**(8), 1223–1245.
24. Vlassak, J. J. and Nix, W. D., Indentation modulus of elastically anisotropic half spaces. *Phil. Magn. A*, 1993, **67**(5), 1045–1056.
25. King, R. B., Elastic analysis of some punch problems for layered medium. *Int. J. Solids Struct.*, 1987, **23**, 1657–1664.
26. Bhattacharya, A. K. and Nix, W. D., Analysis of elastic and plastic deformation associated with indentation testing of thin films on substrates. *Int. J. Solids. Struct.*, 1987, **24**(12), 1287–1298.
27. Saha, R. and Nix, W. D., Effects of the substrate on the determination of thin film mechanical properties by nano-indentation. *Acta Mater.*, 2002, **50**, 23–38.
28. Bobji, M. S. and Biswas, S. K., Hardness of a surface containing uniformly spaced pyramidal asperities. *Tribol. Lett.*, 1999, **7**, 51–56.
29. Qasmi, M., Delobelle, P., Richard, F. and Bosseboeuf, A., Effect of the residual stress on the determination through nano-indentation technique of the Young's modulus of W thin film deposit on SiO_2/Si substrate. *Surf. Coat. Technol.*, 2006, **200**, 4185.
30. Qasmi, M. and Delobelle, P., Influence of the average roughness R_{ms} on the precision of the Young's modulus and hardness determination using nano-indentation technique with a Berkovich indenter. *Surf. Coat. Technol.*, 2006 (in line).
31. Alguero, M., Bushby, A. J., Reece, M. J., Poyato, R., Ricote, J., Calzada, M. J. and Pardo, L., Stress-induced depolarization of (Pb,La)TiO_3 ferroelectric thin films by nano-indentation. *Appl. Phys. Lett.*, 2001, **79**(23), 3830–3832.
32. Devos, A. and Lelouarn, A., Strong effect of interband transitions in the picosecond ultrasonics response of metallic thin films. *Phys. Rev. B*, 2003, **68**, 045405.
33. Goujon, L., *Etude des composites piezoelectriques 1–3 pour applications electroacoustiques sous-marine*, Ph.D. Thesis, 1999, INSA Lyon, France.
34. Guillon, O., *Caracterisation électromécanique et modélisation de céramiques ferroélectriques de type PZT*, Ph.D. Thesis, 2003. Univ. Franche Comté, France.
35. Guillon, O., Thiebaud, F., Delobelle, P. and Perreux, D., Tensile behavior of PZT in short and open conditions. *Mater. Lett.*, 2004, **58**, 986–990.
36. Delafargue, A. and Ulm, F. J., Explicit approximations of the indentation modulus of elastically orthotropic solids for conical indenters. *Int. J. Solids Struct.*, 2004, **41**, 7351–7360.